Magnetized States of Quantum Spin Chains

C. Broholm[1,3], G. Aeppli[2], Y. Chen[1], D. C. Dender[3], M. Enderle[4], P. R. Hammar[1], Z. Honda[5], K. Katsumata[6], C. P. Landee[7], M. Oshikawa[8], L. P. Regnault[9], D. H. Reich[1], S. M. Shapiro[10], M. Sieling[11], M. B. Stone[1], M. M. Turnbull[7], I. Zaliznyak[10], and A. Zheludev[12]

[1] Department of Physics and Astronomy, Johns Hopkins University, Baltimore, MD 21218, USA
[2] NEC Research Institute, 4 Independence Way, Princeton, NJ 08540, USA
[3] National Institute of Standards and Technology, Center for Neutron Research, Gaithersburg, MD 20899, USA
[4] Institute Max Von Laue Paul Langevin, F-38042 Grenoble, France
[5] Faculty of Engineering, Saitama University, Urawa, Saitama 338-8570, Japan
[6] RIKEN Harima Institute, Mikazuki, Sayo, Hyogo 679-5148, Japan
[7] Carlson School of Chemistry and Department of Physics, Clark University, Worcester, MA 01610, USA
[8] Department of Physics, Tokyo Institute of Technology Oh-oka-yama, Meguro-ku, Tokyo, 152-8551 Japan
[9] CEA-Grenoble, DRFMC-SPSMS-MDN, 17 rue des Martyrs 38054 Grenoble cedex 9, France
[10] Physics Department, Brookhaven National Laboratory, Upton, NY 11973, USA
[11] Physikalisches Institut, Universitt Frankfurt, Robert-Mayer-Str.2-4, D-60054 Frankfurt, Germany
[12] Solid State Division, Oak Ridge National Laboratory, Oak Ridge, TN 37831, USA

Abstract. Quantum spin chains display complex cooperative phenomena that can be explored in considerable detail through theory, numerical simulations, and experiments. Here we review neutron scattering experiments that probe quantum spin chains in high magnetic fields. Experiments on copper-containing organometallic systems show that the uniform antiferromagnetic spin-1/2 chain has a gapless continuum of magnetic excitations and is critical in zero field. Application of a magnetic field creates incommensurate soft modes with a characteristic wave-vector that grows in proportion to the magnetization. These experimental results are evidence that the spins-1/2 chain maps to a one dimensional Luttinger liquid. Experiments on antiferromagnetic spin chains built from spin-1 nickel atoms show a Haldane gap to bound triplet excitations and a finite critical field that must be exceeded to induce magnetization at low temperatures. These results indicate that the integer spin chain has an isolated singlet ground state with hidden topological order. For both spin-1/2 and spin-1 systems, site alternation leads to a field induced gap in the excitation spectrum.

1 Introduction

Cooperative phenomena in magnetism generally involve mesoscopic spin clusters with classical dynamics. Consequently, quantum effects are seldom apparent in macroscopic properties. Quasi-one-dimensional magnets are an exception because their long-range correlations are controlled by microscopic domain walls

with quantum dynamics[1]. In these systems, quantum effects can therefore have a profound impact on physical properties on all length scales. Consider for example, a uniform spin chain with antiferromagnetic Heisenberg interactions at $T = 0$. While half odd integer spin chains have quasi-long range order and a gapless spectrum, integer spin chains have a finite correlation length and an isolated singlet ground state[2].

These one-dimensional quantum effects have consequences for macroscopic properties of three-dimensional solids. In particular, there are transition metal oxides and organometallic materials that contain arrays of weakly interacting spin chains. For Cu-spins that represent spin-1/2 degrees of freedom, such an array generally acquires long-range order at sufficiently low temperatures as slowly fluctuating spin chains with quasi-long-range one-dimensional order develop long-range inter-chain phase coherence. However, for quasi-one-dimensional spin systems built from spin-1 Ni atoms, there is a critical value for inter-chain coupling below which low temperature magnetic order cannot be achieved. Systems with sufficiently weak inter-chain coupling adopt a quasi-one-dimensional cooperative singlet ground state at low temperatures without undergoing any phase transitions.

Quantum effects also strongly affect the response of quasi-one-dimensional magnetic systems to an applied magnetic field. For spin chains with a gap in their excitation spectrum, there is a critical field that must be exceeded to induce magnetization at the absolute zero temperature. In addition, the magnetized states of many isotropic quantum spin chains are expected to have incommensurate low energy fluctuations, an effect that has no analogy in magnets with classical dynamics[3].

In this paper, we shall review experiments that probe the magnetized states of uniform antiferromagnetic spin-1/2 and spin-1 chains. The emphasis is on neutron scattering experiments that can provide detailed information about atomic scale dynamic correlations. After a brief summary of the neutron scattering technique, separate sections for spin-1/2 and spin-1 chains describe model systems, zero field data, and finite field data. The experimental results are compared to relevant theories. We end with a summary of results and a discussion of challenges that remain.

1.1 Magnetic Neutron Scattering

Neutrons interact with nuclei through the strong interaction and with electrons through electromagnetic dipole-dipole interactions[4]. The corresponding scattering cross sections for an atom with a partially filled electronic shell are of order r_0^2 for both interactions, $r_0 = (e^2/m_e c^2) = 2.82$ fm being the classical electron radius. The cross sections are sufficiently small that the Born approximation is valid and the scattering processes can be described in terms of a differential scattering cross section. The magnetic part of the cross section, which is of interest here, can be written as follows[5]

$$\frac{d^2\sigma}{d\Omega dE'} = (\gamma r_0)^2 |\frac{g}{2} F(Q)|^2 \sum_{\alpha\beta} (\delta_{\alpha\beta} - \hat{Q}_\alpha \hat{Q}_\beta) \mathcal{S}^{\alpha\beta}(\boldsymbol{Q}, \omega). \tag{1}$$

The scattering process is specified by the wave-vector transfer, $\mathbf{Q} = \mathbf{k_i} - \mathbf{k_f}$ and the energy transfer $\hbar\omega = E_I - E_f$ to the sample. Furthermore, $\gamma = 1.913$ and $g \approx 2$ are the spectroscopic g-factors of the neutron and the magnetic atom respectively, and $F(Q)$ is the magnetic form factor[6]. The interesting part of Eq. (1) is the Fourier transformed two point dynamic spin correlation function:

$$\mathcal{S}^{\alpha\beta}(\boldsymbol{Q}, \omega) = \frac{1}{2\pi\hbar} \int dt e^{i\omega t} \frac{1}{N} \sum_{\boldsymbol{R}\boldsymbol{R}'} < S^\alpha_{\boldsymbol{R}}(t) S^\beta_{\boldsymbol{R}'}(0) > e^{-i\boldsymbol{Q}\cdot(\boldsymbol{R}-\boldsymbol{R}')} \tag{2}$$

$\mathcal{S}^{\alpha\beta}(\boldsymbol{Q}, \omega)$ can be be related to the generalized spin susceptibility through the fluctuation dissipation theorem[5].

$$\mathcal{S}(\boldsymbol{Q}, \omega) = \frac{1}{1 - e^{-\beta\hbar\omega}} \frac{\chi''(\boldsymbol{Q}, \omega)}{\pi (g\mu_B)^2} \tag{3}$$

where $\beta = 1/k_B T$ and χ'' denotes the imaginary part of the generalized spin susceptibility. $\mathcal{S}(\boldsymbol{Q}, \omega)$ is the natural juncture for theoretical and experimental work on cooperative magnetic phenomena and magnetic neutron scattering is the experimental technique that provides the most complete access to it.

Many of the neutron scattering experiments to be described in this article were performed on the SPINS cold neutron spectrometer at the NIST Center for Neutron Research, which is shown in Fig. 1. Neutrons from the cold

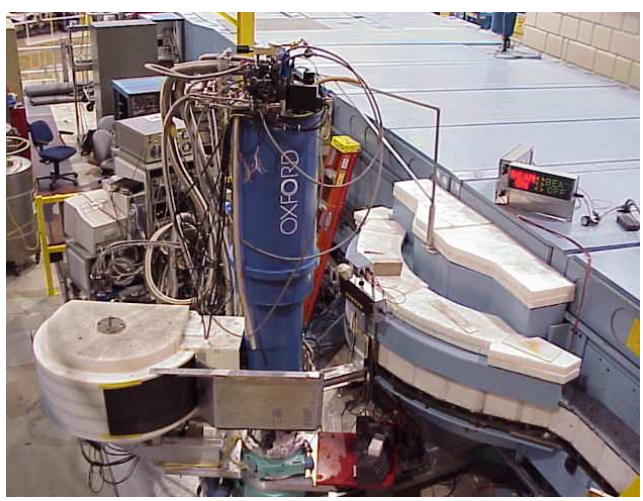

Fig. 1. The SPINS cold neutron spectrometer at the NIST Center for Neutron Research in Gaithersburg, MD, USA where many of the experiments described in this paper were performed. The tall cylindrical item marked Oxford, is a high field dilution refrigerator.

source of the 20 MW NBSR reactor are transported to the instrument through an evacuated rectangular glass structure with inner dimensions 6 cm by 12.5 cm. The inner walls of this neutron guide are coated with ^{58}Ni, which completely reflects neutrons with an angle of incidence less than a critical angle $\theta_c = 2.04 \cdot 10^{-3}\text{Rad/Å} \times \lambda$, where λ is the neutron wave-length. A horizontally segmented pyrolytic graphite monochromator Bragg reflects a monochromatic and vertically focused beam to the sample position. The incident beam energy range is 2.3 meV to 14 meV and the relative energy resolution 2-8% depending on the configuration. The neutron beam easily penetrates the aluminum vacuum cans of cryogenic systems that provide appropriate thermodynamic conditions for the sample.

The detection system is contained within a shielded volume to reduce background contributions from epithermal neutrons. The neutron detector is a ^{3}He proportional counter with greater than 90% detection efficiency for neutrons with energies less than 15 meV. To reach the detector, neutrons scattered from the sample must reflect from a pyrolytic graphite crystal. This ensures that, the energy of detected neutrons is known by virtue of the fact that they must have satisfied the Bragg conditions at this "analyzer" crystal. The SPINS instrument offers much flexibility in configuring the detection system. In particular, the analyzer consists of 11 vertical blades with a height of 15 cm and widths of 2.1 cm that can rotate independently about vertical axes. The analyzer is placed 91 cm from the sample where it can rotate about a vertical axis. The entire detection system in turn can rotate about the sample to access neutrons scattered in different directions by the sample.

We used three basic detector configurations for the experiments reported here. In the conventional "triple axis" mode, Soller collimators surrounding the analyzer determine the scattering angle at the analyzer. Only three vertical analyzer blades are used in this mode and the detector is then sensitive only to a specific fixed neutron energy. To vary energy transfer, the incident beam energy is changed by adjusting the scattering angle at the monochromator.

In the monochromatic focusing mode the final energy is also fixed, however, the eleven blades of the segmented analyzer are set up to reflect neutrons with a range of scattering angles from the sample onto a single channel detector. The loss of wave-vector resolution perpendicular to the direction of the scattered beam is not a problem for one-dimensional systems as the chain axis can be oriented along $\mathbf{k_f}$ where the wave-vector resolution is excellent. The monochromatic focusing mode enhances sensitivity by approximately a factor five over the conventional triple axis configuration without increasing the fast neutron background. It requires a weakly dispersive direction for the system of interest and a single crystalline sample with low mosaic distribution.

The third configuration that we use is denoted the energy dispersive analyzer mode. All analyzer blades are oriented parallel to the analyzer assembly so they form a flat reflecting surface that subtends a solid angle of approximately 0.04 Sr to the sample. Neutrons with varying sample scattering angles also have different angles of incidence on the analyzer and hence the Bragg condition for reflection

varies across the surface of the analyzer. The beam reflected from the analyzer in this mode has a horizontal divergence angle of approximately 10 degrees. After passage through a radial collimator for background suppression, neutrons are detected by a position sensitive detector. Splayed horizontally over the detector are thus neutrons corresponding to a range of different values of $\mathbf{Q}$ and $\hbar\omega$, with $\mathbf{Q}$ varying along the reciprocal lattice direction defined by the analyzer surface. The dispersive analyzer mode enhances efficiency by approximately a factor five over the conventional triple axis mode. Background tends to be higher than for the monochromatic focusing mode but the configuration can be used for samples that are dispersive throughout the horizontal plane or where the sample mosaic distribution covers several degrees.

2 Antiferromagnetic Spin-1/2 Chain

The uniform antiferromagnetic spin-1/2 chain plays a special role in physics because it is one of very few interacting quantum many body system, where exact analytical results are available. The spin Hamiltonian reads

$$\mathcal{H} = J \sum_n \mathbf{S}_n \cdot \mathbf{S_{n+1}} - g\mu_B H \sum_n S_n^z, \tag{4}$$

where $J > 0$ is the antiferromagnetic exchange constant and $\mathbf{S}_n$ are vector spin operators for spin-1/2 degrees of freedom.

2.1 Theoretical results for the spin-1/2 chain

There is a steadily growing body of exact results available about the uniform spin-1/2 chain, most of them based on the Bethe ansatz[7,8]. This correct "guess" for the ground state of the spin-1/2 chain enabled calculation of the ground state energy per spin in the absence of a magnetic field[9] $< \mathcal{H} > /N = |J|2(\frac{1}{4} - \ln 2)$. Bethe's ansatz was later used to derive thermodynamic properties including the equal time spin correlation function

$$\langle \mathbf{S}_i \cdot \mathbf{S}_{i+n} \rangle = (-1)^n n^{-1}, \tag{5}$$

which indicates quasi-long-range antiferromagnetic order. It is also possible to derive the wave functions and energies for the lowest energy excited states as a function of wave-vector transfer[10]:

$$\epsilon_L(q) = \frac{\pi}{2} J |\sin q| \tag{6}$$

The functional form of this expression is similar to the dispersion relation for spin waves in a putative spin-1/2 one-dimensional antiferromagnet with exchange constant $\pi J/2$. However, Eq. 6 is not the dispersion relation for a long lived quasiparticle, rather it represents the lower bound of a continuum of excited

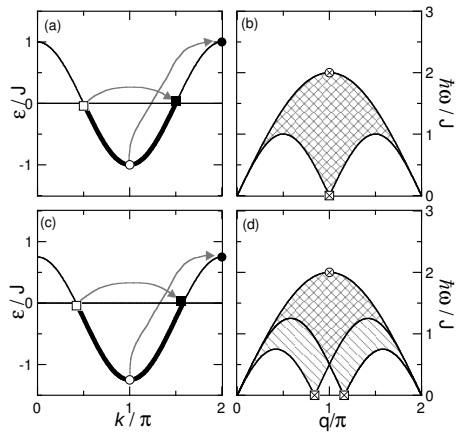

Fig. 2. Exact zero and finite field results for the XY spin-1/2 chain obtained through the Jordan-Wigner transformation. The Heisenberg spin chain has qualitatively similar properties as described in Ref. [14]. (a) Shows the band structure for spinons in the unmagnetized state. (b) shows the corresponding exact kinematical limits of the two spinon continuum. Arrows in (a) indicate scattering processes that map to the points on frame (b). (c) shows the band structure for spinons in a magnetized state. The exact boundaries [14] of the corresponding continuum in the longitudinal part of the dynamic spin correlation function, $\mathcal{S}^{\ddagger\ddagger}(q,\omega)$, are shown in (d). The transverse part of the dynamic spin correlation function is gapless for $q = \pi$.

states. It has been shown that the fundamental quasi-particles of the spin-1/2 chain are fermionic "spinons" that occupy a cosine band[11,12]

$$\epsilon(q) = \frac{\pi}{2} J \cos q. \tag{7}$$

For the easy plane spin-1/2 chain, spinons do not interact and thus they form an ideal one-dimensional degenerate fermi gas[13]. For isotropic interactions (the Heisenberg case), there are strong interactions and spinons form a one-dimensional Luttinger liquid. For the un-magnetized spinchain, the spinon band is half filled as indicated in Fig. 2(a). Low energy excitations with wave-vector transfer, q, correspond to annihilating a spinon with wave-vector $q_1 \approx n\pi$ and creating a spinon with wave-vector $q_2 = n\pi + q$. Arrows in Fig. 2(a) indicate such spinon scattering processes while points in Fig. 2(b) indicate the corresponding values of wave-vector and energy transfer. The solid lines in Fig. 2(b) indicate the kinematical limits for spinon excitations.

Neutron scattering can probe the kinematical limits of the spinon excitation spectrum. The experiments are also sensitive to the matrix elements for spin excitations. Specifically, the dynamic spin correlation function measured by neutron scattering at zero temperature can be written as

$$\mathcal{S}^{\mu\mu}(q,\omega) = 2\pi \sum_{\lambda} | < 0|S_q^{\mu}|\lambda > |^2 \delta(\hbar\omega - (\epsilon_\lambda - \epsilon_0)) \tag{8}$$

Recent mathematical breakthroughs have enabled analytical calculation of this important quantity for the dominant two spinon excitations in zero magnetic field[8].

Because an (un)occupied spinon state represents a spin up (down) the magnetized spin-1/2 chain maps to a spinon band away from half filling as shown in Fig. 2(c). Fig. 2(d) shows the corresponding kinematical limits for low energy excitations, which are significantly more complicated than for the unmagnetized state. The principal feature of interest, are the low energy incommensurate modes of excitation with wave-vectors that are related to the magnetization as follows

$$q_i = n\pi \pm 2\pi < S_z > \tag{9}$$

The field induced incommensurate modes have an alternate phenomenological interpretation. As the incommensurate modes are gapless, they represent a spin density modulation that persists on an arbitrarily long time scale. The magnitude of the incommensurate wave-vector further indicates that the magnetization is carried by magnetized defects in quanta of spin-1/2 and with density $\rho = 2 < S_z >$. The band versus "defect lattice" description of the magnetized spin-1/2 chain can be compared to the band versus striped model for the incommensurate spin correlations in the copper oxide two-dimensional lattice of high temperature superconductors[15,16].

Chemical Formula	Common Name	J (meV)	T_N (K)	$g\mu_B H/J$	$\sigma_{\rm inc}$ barn	Refs.
$SrCuO_2$		280(20)	<1.5	0.007	0.61	[17–19]
Sr_2CuO_3		260(10)	5	0.006	0.67	[18,20–23]
Ca_2CuO_3		≈86	8	0.013	0.65	[24,25]
$BaCu_2Ge_2O_7$		46.5	8.5	0.024	0.808	[26,27]
$BaCu_2Si_2O_7$		24.1	9.2	0.048	0.632	[26,28–30]
$KCuF_3$		17.5	39	0.067	0.82	[31–35]
$CuGeO_3$		10.4	$T_{SP} = 14$	-	0.73	[36–38]
$CuCl_2 \cdot 2N(C_5H_5)$	CPC	2.31	1.14	0.50	110.9	[39,40]
$Cu(C_6H_5COO)_2 \cdot 3(H_2O)$	Cu-Benzoate	1.57	0.8	0.73	158.5	[41,42]
$[(CH_3)_2SO_2]CuCl_2$	CDC	1.43	0.91	0.81	70.4	[43,44]
$Cu(C_4H_4N_2)(NO_3)_2$	CuPzN	0.90(1)	<0.05	1.29	42.0	[45]
$CsCuCl_4$		0.34(2)	0.62	3.40	22.0	[46]
$CuSO_4 \cdot 5(H_2O)$		0.25	0.100	4.63	99.3	[47,48]
$CuSeO_4 \cdot 5(H_2O)$		0.15	0.125	7.72	99.6	[47,48]

Table 1. Key characteristics of S=1/2 linear chain Heisenberg antiferromagnets ordered according to the magnitude of the exchange constants. T_N refers to the temperature below which long range magnetic order develops. T_{SP} indicates the critical temperature for a spin-Peierls transition. $g\mu_B H/J$ is calculated with $g = 2$ and $H = 10$ Tesla. The incoherent cross section, $\sigma_{\rm inc}$, is in units of 10^{-24}cm^2 per spin-1/2. Further tabulations of S=1/2 HAFM chains can be found in references [49] and [50].

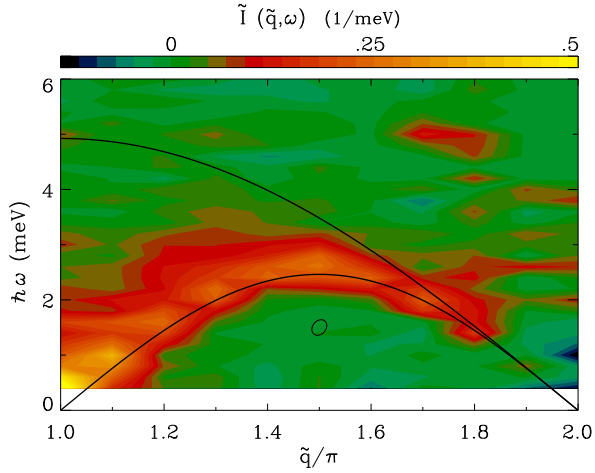

Fig. 3. Image of the dynamic spin correlation function for the spin-1/2 chain copper benzoate in the non-magnetized state. The ellipsoid shows the half width at half maximum instrumental resolution. Reproduced from Ref.[42]

2.2 Experimental Model Systems

To examine spin correlations in the one-dimensional spin-1/2 chain through experiments requires suitable model systems that faithfully realize the spin-hamiltonian in Eq. 4. Table 1 lists some of the materials that have served as model experimental systems. It is important that the ordering temperature is small compared to the exchange constant as that indicates a highly one-dimensional materials where inter-chain interactions can be neglected for $\hbar\omega > k_B T_N$. The absolute value of the exchange constant determines the experimental conditions that are necessary to access a certain range of normalized temperature $k_B T/J$, normalized field $g\mu_B H/J$, and normalized energy transfer, $\hbar\omega/J$. For the present work, we are interested in large values of normalized magnetic field in the $\approx$ 10 T superconducting magnets that are available for neutron scattering experiments. At the same time, we want to resolve the magnetic excitation spectrum using a cold neutron triple axis spectrometer with energy resolution of order 0.1 meV. This implies an exchange constant, $J \approx 1$ meV. To optimize the signal to noise ratio it is desirable to minimize the nuclear incoherent scattering cross section per magnetic ion, a quantity also listed in the table. The two model systems that we shall focus on in this article are copper benzoate ($Cu(C_6H_5COO)_2 \cdot 3(H_2O)$) and copper pyrazine dinitrate ($Cu(C_4H_4N_2)(NO_3)_2$). Both are highly one-dimensional and have exchange constants small enough to enable large values of the reduced magnetic field. One difference that will turn out to be important for the high field experiments is that copper benzoate has two magnetic atoms per one-dimensional unit cell, while copper pyrazine dinitrate has only one.

2.3 Zero Field Properties

The zero field dynamic spin correlation function for the spin-1/2 chain was measured using cold neutron scattering from copper benzoate and is shown in Fig. 3. Similar data are also available for $KCuF_3$[51] and copper pyrazine dinitrate[52]. While most of the intensity is accumulated along the lower boundary of the two spinon continuum (Eq. 6), the distribution is significantly wider than can be accounted for by the instrumental resolution function (solid ellipse). The data is instead consistent with a bounded two spinon continuum.

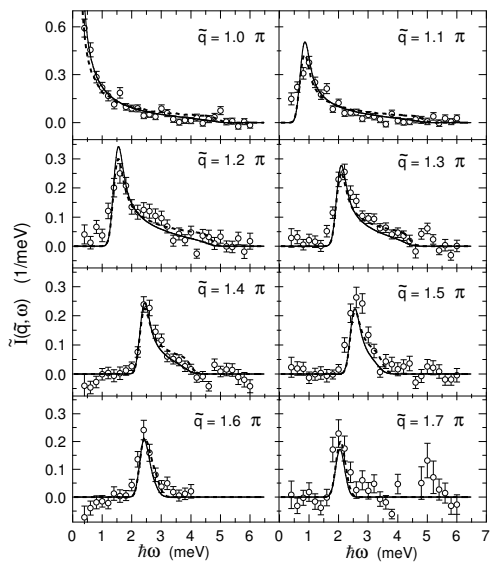

Fig. 4. Constant wave-vector cuts through the zero field neutron scattering data for copper benzoate shown in Fig. 3. The solid lines show the resolution convoluted exact two spinon contribution to the dynamic structure factor. The dashed line shows the resolution convoluted Müller approximation. Just two parameters were extracted from the combined data set. An overall pre-factor and the exchange constant $J = 1.57(1)$ meV. Adapted from Ref.[42]

Comparison to theories of the detailed energy dependence of the dynamic spin correlation function is best accomplished by comparing cuts through the data to resolution convoluted intensity distributions as shown in Fig. 4. The dashed lines show a phenomenological approximation that provides a good fit to the data[14,53]. The exact two spinon contribution to the dynamic spin correlation function shown with the solid line is difficult to distinguish from the approximate model[54]. The distinction lies in the higher energy part of the spectrum where the exact two spinon contribution to $\mathcal{S}(q, \omega)$ falls off more smoothly than the phenomenological form.

2.4 Spin correlations in the Magnetized State

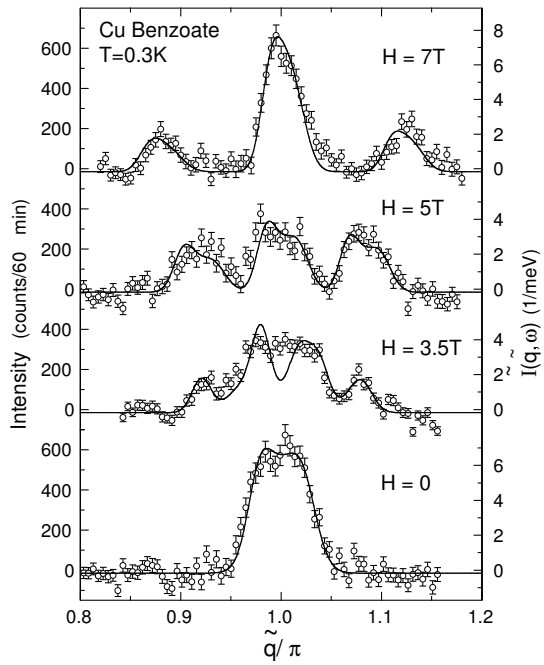

Fig. 5. Constant energy scans for $\hbar\omega = 0.21$ meV at various values of applied magnetic field at $T = 0.3$ K for copper benzoate. The data show the development of incommensurate soft modes in the magnetized spin-1/2 chain. Solid lines show a resolution convoluted model calculation as described in Ref.[41].

We now turn to the experimental evidence for incommensurate spin correlations in the magnetized state of the spin-1/2 chain. Fig. 5 shows constant energy scans at low energies ($\hbar\omega/J = 0.13$) and for values of the applied field ranging from 0 to $g\mu_B H/J = 0.51$. At zero field the data provide clear evidence for a two spinon continuum since long lived spin wave excitations would give rise to two resolution limited peaks rather than a single flat top maximum.

At finite field two small peaks split off symmetrically about $q = \pi$ and move progressively further from this location with increasing applied field. From these data, we derived the field dependence of the soft mode wave-vector that is plotted in Fig. 6. The solid line in the figure is based on Eq. 9 and a calculation of the field dependent magnetization of the spin-1/2 chain. Clearly, the wave-vector dependence of the quasi-one-dimensional soft modes in copper benzoate is consistent with the spinon theory for the uniform spin-1/2 chain. However, while the theory predicts a gapless spectrum Fig. 6(b) shows that there is a field-induced gap for copper benzoate.

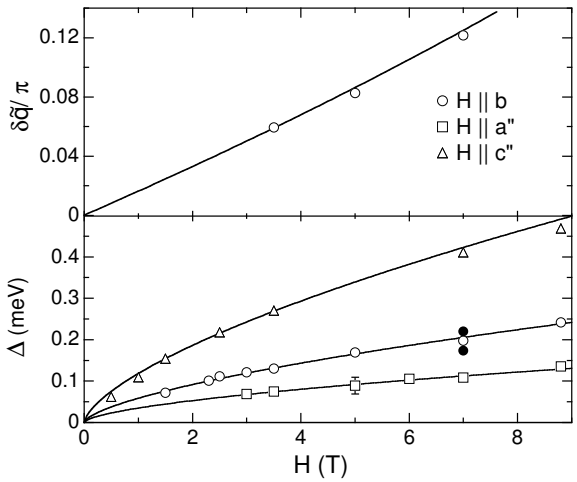

Fig. 6. (a) Field dependence of the incommensurate wave-vector for low energy spin excitations in the spin-1/2 chain copper benzoate. (b) Field dependence of the gap in the excitation spectrum of same material from a combination of neutron scattering and specific heat data. Reproduced from Ref. [41].

Exchange anisotropy that defines an easy plane parallel to the field direction could in principle account for the gap as application of a magnetic field creates an easy axis perpendicular to the field. However, the magnitude of exchange anisotropy in copper benzoate can be estimated from the g-tensor anisotropy to be of order 1%, which is insufficient to account for the magnitude of the field induced gap[55]. Instead, it appears that staggering of the g-tensor along the spin chain as well as an alternating Dzyaloshinski-Moriya interaction causes the field-induced gap[56,57]. While neither of these terms have significant impact on zero field properties, they lead to unit cell doubling in a field and transverse long-range antiferromagnetic order. Because low energy excitations in the spin-1/2 chain correspond to a sliding spin density wave, the formerly gapless two-spinon continuum acquires a gap when odd and even sites of the spin chain become distinguishable in a field. In field theoretical language, a staggered field is a relevant perturbation for the spinon Luttinger liquid. It can readily be shown using bosonization techniques that a staggered field induces a gap in the excitation spectrum that grows in proportion to H_s^α, where $\alpha = 2/3$ in the limit of a small staggered field, H_s and a small uniform field[56]. As the staggered g-tensor induces a transverse staggered field in proportion to the uniform field the result is a spin gap that grows in proportion to the applied field to this same power $\alpha \approx 2/3$. The solid line in Fig. 6(b) is a power-law fit that yields $\alpha_{exp} = 0.65(3)$, a value that is in excellent agreement with the theory.

It has been shown that the effective low energy theory for a spin-1/2 chain with a staggered field is the Sine-Gordon model[56–58]. Originating as a mathematical model in particle physics, this model has been used to analyze condensed

matter systems ranging from one-dimensional Josephson Junctions to quasi-one-dimensional easy-plane ferromagnets. However, the spin-1/2 chain with a staggered field may prove to be the best system yet in which to explore the rich excitation spectrum of this model through experiments[57].

It is interesting to note that despite the transition from a gapless spinon Luttinger liquid to a gapfull Sine-Gordon model, the field dependent incommensurability is perfectly accounted for by Eq. 9. This indicates that the appearance of incommensurate soft modes in magnetized quantum spins is a general phenomenon that should find a general explanation. One possibility is that magnetization is carried by repulsive defects in the zero field singlet ground state much as flux is carried by flux lines in the mixed phase of type II superconductors[3].

The existence of such repulsive defects (alias solitons) is well demonstrated in the spin-1/2 Heisenberg chain in presence of sizable spin-lattice couplings. In that case, the 3D lattice undergoes a structural instability induced by the magnetic fluctuations below a well-defined temperature T_{SP}, the so-called spin-Peierls transition temperature. Consequently, the chains dimerize, giving rise to a non-magnetic singlet ground state and an energy gap $\Delta_{SP} \approx 1.74 k_B T_{SP}$ opens in the excitation spectrum at $q = \pi$ [59]. Under field, the spin-Peierls system undergoes a transition to an incommensurate magnetic phase at a critical field H_C directly related to Δ_{SP} [60,61]. In the high-field phase, a soliton lattice forms, with both structural and magnetic components characterized by an incommensurate (IC) wave-vector shifted from $q = \pi$ by a quantity $\delta k_{SP} \propto < S_z >$. Neutron diffraction measurements on $CuGeO_3$ have provided direct evidence for a long-ranged dual (magnetic and structural) soliton structure above $H_C \approx 12.5$ T [62]. Figure 7 shows the field dependences of δk_{SP} and the soliton width Γ, compared to the field-theory prediction [60] and to x-ray data [63]. Contrary to the pure Heisenberg chain, incommensurate excitations exist only above H_C for the spin-Peierls system [64].

3 Uniform Antiferromagnetic Spin-1 Chain

Haldane discovered that integer spin chains are qualitatively different from half odd integer spin chains[2,65,66]. His approach was a large S mapping of the spin Hamiltonian to the $O(3)$ non-linear sigma model with a topological term associated with the Berry phase of the spin. For integer spins the topological term vanishes, while for half odd integer spins the topological term is important. When there is no topological term the non linear sigma model maps to a classical two-dimensional ferromagnet at finite temperature. This model has short-range order, which implies short-range order for the integer spin chain as well. For the half odd integer spin chain however, the topological term leads to a variant of the sigma model with instanton quark confinement and a gapless excitation spectrum consistent with the results described above[65].

Given the fact that the sigma model mapping relies on $S \to \infty$ one might question the applicability of results derived from it for spin chains with $S \leq 1$. While there are certainly quantitative differences, there are arguments against

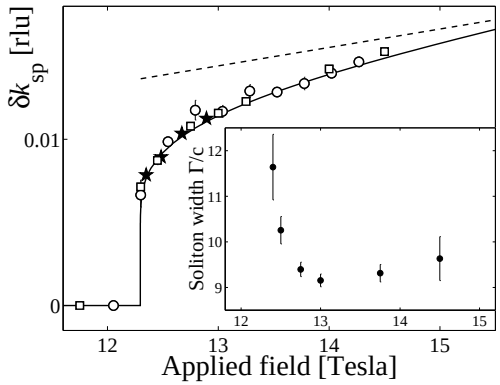

Fig. 7. Field dependence of the incommensurate component of the wave-vector (δk_{SP}) and soliton width Γ in the high-field phase of $CuGeO_3$. Open symbols: Neutron diffraction. Stars: X-ray data [63]. The lines are calculated curves according to the theories of Buzdin *et al.* [60] (solid line), and Cross *et al.* [59] (dashed line).

qualitative changes in the behavior of integer spin chains as S becomes smaller such that the main conclusions derived from the $S \to \infty$ mapping should persist in the small S limit. In addition, there are various other theoretical and numerical results that support a gap for integer spin chains. One is the Lieb Schultz Mattis theorem, which states that a gap can only be present in a quantum spin chain if the spin quantum number per unit cell is integral[67–69]. There is also much numerical work, which provides compelling evidence for spin gaps in integer spin chains[70,71].

A simple explanation for a spin gap in the spin-1 chain was provided by Affleck, Kennedy, Lieb, and Tasaki[72]. They identified a valence bond solid state in which each of the spin-1/2 degrees of freedom that in pairs make up atomic spin-1 are contracted with neighboring spin-1/2 degrees of freedom to form a singlet. Such valence bond solid states are possible when twice the spin quantum number matches the nearest neighbor coordination number. The valence bond solid for a spin-1 chain is the exact ground state of a projection spin hamiltonian of the following form

$$\mathcal{H}'_{VBS} = \sum_n P_2(\mathbf{S}_n, \mathbf{S}_{n+1}), \tag{10}$$

The projection operator, P_2, is unity when the argument spin operators combined form a spin-2 degree of freedom and zero otherwise. Clearly the ground state for $\mathcal{H}'_{VBS}$ has no near neighbor spin pairs in a spin 2 state and this exactly defines the valence bond solid state. Projection operators can in general be expanded as a power series of order $2S$ in spin dot products[73]. In particular, for spin-1 the spin-2 pair projection operator takes the form

$$P_2(\mathbf{S}_i, \mathbf{S}_j) = \frac{1}{2}\mathbf{S}_i \cdot \mathbf{S}_j + \frac{1}{6}(\mathbf{S}_i \cdot \mathbf{S}_j)^2 + \frac{1}{3} \tag{11}$$

Thus the hamiltonian that has the valence bond solid ground state can be written in terms of spin-1 operators as follows :

$$\mathcal{H}_{VBS} = \sum_n \left[\mathbf{S}_n \cdot \mathbf{S}_{n+1} - \beta (\mathbf{S}_n \cdot \mathbf{S}_{n+1})^2 \right], \tag{12}$$

where $\beta = -1/3$ and trivial terms and factors have been removed for simplicity. Studies of this hamiltonian as a function of β indicate that there are no phase transitions at $T = 0$ as β is driven to zero. The implication is that the valence bond solid is a good initial ansatz for describing the conventional Heisenberg spin-1 chain itself. Of course these arguments only hold for the spin-1 case. In particular, for spin-1/2 the condition that $2S$ equals the number of nearest neighbors is not fulfilled so that a valence bond solid state is not possible in that case.

The valence bond solid state for an even length chain with $\beta = -1/3$ can be written as follows[74]

$$|\Psi_{VBS}>= \sqrt{2}|000...> + \sum_{m=2,4,6,...} 2^{(m-1)/2} \sum_{perm} |0+0-0+0-00+00-...> \tag{13}$$

where m counts the number of sites with projection quantum numbers different from 0 and the superposition is over all states where removal of sites with no spin projection along the quantization axis leaves behind a perfectly ordered m-site Néel state. A similar exact ground state wave function can be written for odd length chains. The valence bond solid is accordingly said to have perfect string order. String order is gauged by the expectation value of the following non-local operator

$$\mathcal{O}_{jk} = S_j^z \exp(i\pi \sum_{n=j}^{k-1} S_n^z) S_k^z \tag{14}$$

$\mathcal{H}_{VBS}$ has perfect long range string order: $\lim_{|j-k|\to\infty} < \mathcal{O}_{jk} >_{VBS} = \frac{4}{9}$. It has been shown that there is also long range string order in the spin-1 chain with $\beta = 0$ though the value of the order parameter is reduced to approximately 0.37[75].

Excited states of the spin-1 chain correspond to breaking a valence bond in the valence bond solid state[76]. Broken valence bonds can propagate coherently through the string ordered phase where they only scatter from other string order defects. Creation of a broken valence bond at rest requires an energy of $\Delta = 0.41050(2)J$ for the bi-linear spin-1 chain ($\beta = 0$)[71].

Owing to the isolated singlet ground state of the spin-1 chain and the gap in the excitation spectrum, there is also a minimum critical field $H_c = \Delta/g\mu_B$ required to magnetize the system. Above the critical field there is a gapless critical phase[77] that could have similarities to the magnetized state of the spin-1/2 chain[3]. One of the goals of the present research has been to explore the possibility of incommensurate spin correlation in this magnetized phase of the spin-1 chain.

3.1 Experimental Model Systems

Table 2 contains key characteristics of experimental model systems for the Haldane spin-1 chain. As opposed to the spin-1/2 chain, a spin-1 degree of freedom is affected by single ion anisotropy. This turns out to be a greater obstacle to finding good model system than interchain coupling. While single ion anisotropy splits the triplet excited state, inter-chain coupling must exceed a threshold of order the Haldane gap energy to have a significant impact on the properties of a spin-1 chain. Here we shall focus on NENP and NDMAP for which high field experiments have been performed. We shall see that the materials have very different behavior in a field owing to g-factor alternation, which is present in the case of NENP but absent for NDMAP.

Chemical Formula	Common Name	J meV	$\lvert J'/J\rvert$ 10^{-3}	D/J 10^{-3}	T_N K	$g\mu_B H/J$	Reference
$AgVP_2S_6$		58(4)	0.01	5.8	< 2	0.020	[78]
Y_2BaNiO_5		21	< 0.5	-39	< 0.05	0.055	[79–81]
$Ni(C_3H_10N_2)_2N_3(ClO_4)$	NINAZ	10.7	< 0.7	170	< 0.06	0.11	[82–84]
$Ni(C_3H_10N_2)_2NO_2(ClO_4)$	NINO	4.5		250	< 1.2	0.21	[85,86]
$Ni(C_2H_8N_2)_2NO_2(ClO_4)$	NENP	4.1(3)	0.8	180	< 0.0003	0.28	[87–89]
$Ni(C_5D_{14}N_2)_2N_3(PF_6)$	NDMAP	2.85	0.6	250	< 0.25	0.41	[90–94]
$CsNiCl_3$		2.275	17	-1.9	4.9	0.45	[103,95,96]

Table 2. Key characteristics of quasi-one-dimensional $S = 1$ Haldane antiferromagnets. $g\mu_B H/J$ is calculated with $g = 2$ and $H = 10$ Tesla.

3.2 Zero Field Properties

A comprehensive map of the zero field excitation spectrum for the Haldane spin-1 chain has been obtained through neutron scattering experiments on NENP[87,88,100]. Figure 8(a) shows the zero field dispersion relation for long lived magnetic excitations. The absence of reflection symmetry about the $q = \pi/2$ line indicates that translation symmetry remains identical to the paramagnetic phase for $T << J/k_B$ despite antiferromagnetic interactions. Figure 8(b) shows the wave-vector dependence of the energy integrated intensity, which is a measure of the equal time spin correlation function. For a spin system with long lived excitations, the dispersion relation and equal time spin correlation function are related through an exact sum-rule[101]. Specifically it can be shown that,

$$\mathcal{S}^{\alpha\alpha}(q) = \hbar \int_{-\infty}^{\infty} \mathcal{S}^{\alpha\alpha}(q,\omega) d\omega \tag{15}$$

$$\simeq \frac{\hbar}{\omega^{\alpha\alpha}(q)} \int_{-\infty}^{\infty} \omega \mathcal{S}^{\alpha\alpha}(q,\omega) d\omega \tag{16}$$

$$\simeq -\frac{2}{3} \frac{< \mathcal{H} > /L}{\hbar\omega^{\alpha\alpha}(q)} (1 - \cos q) \tag{17}$$

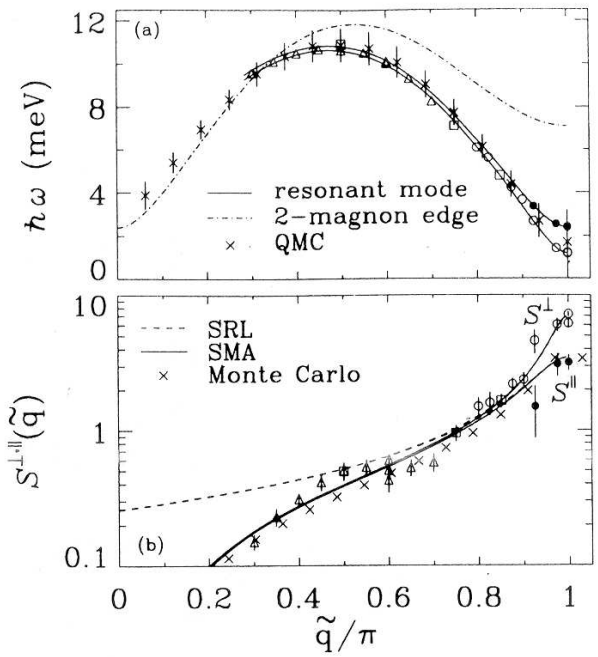

Fig. 8. (a) Circles, triangles, squares, and solid lines: dispersion relation $\omega(q)$ for long-lived modes in NENP. Dot-dashed line: Lower edge of corresponding two-magnon continuum. Crosses: QMC results [97] scaled by $J = 4.1$ meV. (b) Instantaneous spin correlation function $\mathcal{S}^{\perp,\parallel}(q)$. Crosses: Monte Carlo results [98,99]. Dashed lines: square-root Lorentzians with $\xi = 8.5$ and 4.2. Solid lines: single mode approximation based on $\omega(q)$. In both (a) and (b), open and filled symbols for $q > 0.9\pi$ correspond to polarizations perpendicular and parallel to the chain.

where $< \mathcal{H} > /L$ is the ground state energy per spin. The solid line in Fig. 8(b) shows that this so called single mode approximation[102] provides an excellent account of neutron scattering data through most of the zone. Subsequent higher resolution data for $CsNiCl_3$ show spin wave damping setting in for $q < \pi/2$[103].

Figure 9 shows an energy scan at $q = \pi$ for NDMAP in zero magnetic field. The data illustrate the effects of strong easy plane anisotropy in this material. The upper mode corresponds to spin fluctuations polarized along the spin chain, while the lower peak consists of two near degenerate excitations that are polarized in the perpendicular plane. These three modes would be degenerate for an isotropic system but for NDMAP they are split by single ion and/or exchange anisotropy. The solid lines in the figure were calculated based on the SMA and the known resolution of the neutron scattering spectrometer.

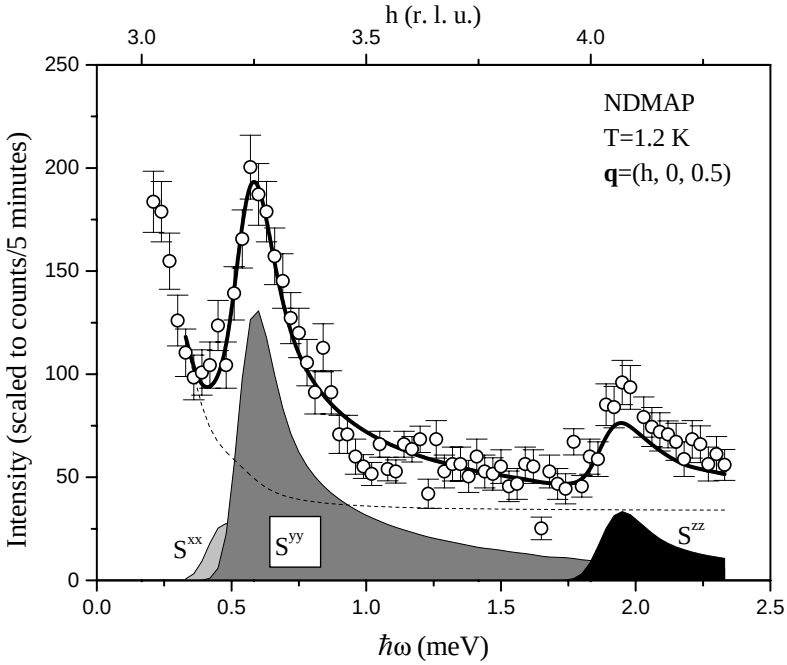

Fig. 9. Constant $q = \pi$ scan in NDMAP at zero field and T=0.3 K. The data was collected with a horizontally focusing analyzer so the spin chain was oriented along the scattered beam direction throughout the scan. x, y, and z refer to the a, b, and c directions respectively of the orthorhombic structure. The solid lines were calculated based on the SMA and known resolution effects. Reproduced from Ref. [92]

3.3 Spin correlations in the Magnetized State

Figure 10 shows the field dependence of excitations at $q \approx \pi$ in NENP for fields applied along the **c** axis[104]. There are two Ni atoms per unit cell along the spin chains in this material so just like in copper benzoate, application of a uniform external field implies that the spin system effectively is also subject to a staggered field. The staggered field immediately induces transverse long range antiferromagnetic order as was clearly observed through neutron diffraction[17] and ESR[105]. In addition, a staggered field is a relevant perturbation on the high field gapless phase of the ideal Haldane spin chain. It is apparent from Figure 10, that NENP does not have a finite field phase transition from a gap-full to a gap-less phase. Rather there is induced Néel order at any finite field and a cross over from a low field phase with a Haldane gap to a high field phase with a gap induced by the staggered field.

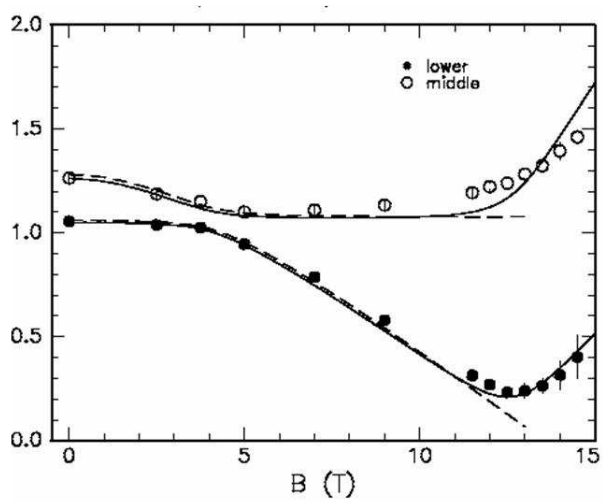

Fig. 10. Field dependence of the energies of easy $\mathbf{a}-\mathbf{c}$ plane excitation at $q \approx \pi$ in NENP for fields applied along the **c** direction at $T = 0.3$ K. In zero field the upper mode shown with open circles is polarized along the **a**-direction. Reproduced from Ref. [104].

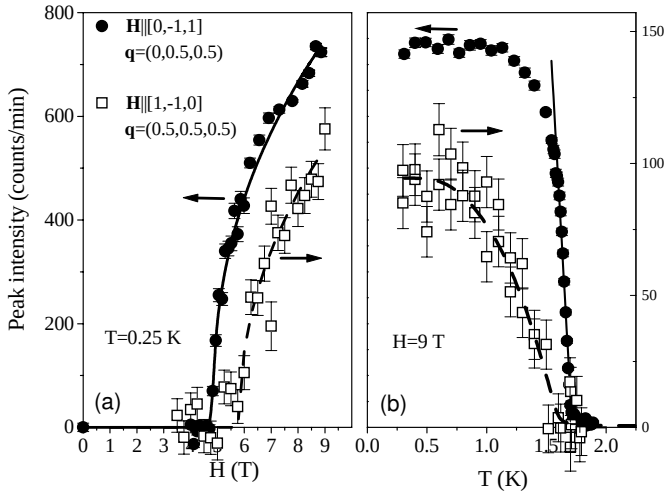

Fig. 11. Field and temperature dependence of elastic magnetic scattering in NDMAP close to the critical field. Field and wave-vectors are indicated on the figure. Only for fields with a component along the hard **c** axis do we find three-dimensional long-range order. The open circles recorded for fields in the easy plane measure the intensity of Bragg rods that correspond to quasi-two-dimensional magnetic order. Reproduced from Ref. [91]

As a model system for studying the magnetized Haldane spin chain, NDMAP has the advantage that there is only one Ni-site per unit cell along the spin chain. Consequently it is possible to apply a pure uniform magnetic field. Figure 11 shows that NDMAP has a bona-fide critical phase transition at a finite field. As a consequence of inter-chain interactions, the ordered phase persists to finite temperatures. A critical field induced phase transition has also been found in the spin-1 chain NDMAZ[106]. Interestingly, the nature of the ordered phase in NDMAP appears to be strongly dependent on the direction of the applied magnetic field. For fields applied strictly in the easy plane, the elastic magnetic scattering in the high field phase takes the form of rods in reciprocal space rather than resolution limited Bragg peaks. This indicates quasi-two-dimensional magnetic order. However, when the field has a component along the hard chain axis, there are resolution limited Bragg peaks indicating long range magnetic order. The high field phase diagram also is highly anisotropic and indicates qualitatively different cooperative properties for fields parallel and perpendicular to the chain axis[107,108].

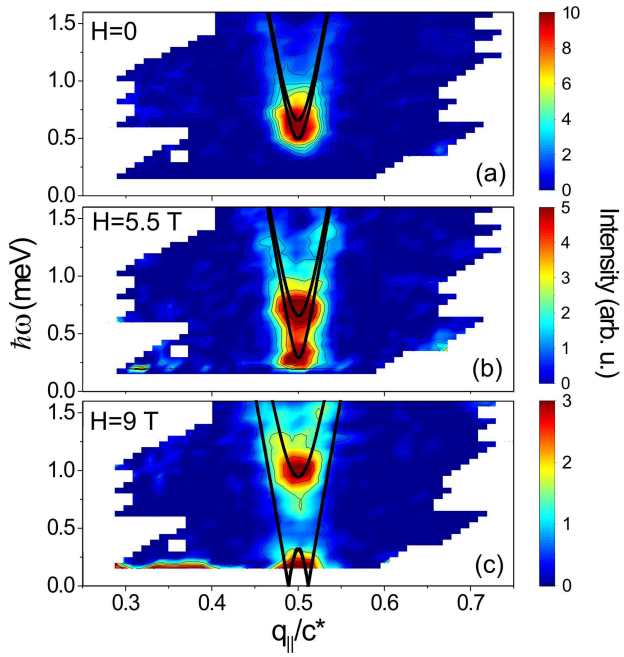

Fig. 12. Inelastic magnetic neutron scattering measured in NDMAP at $T = 2.5$ K for different values of magnetic field applied along the b axis. The extra intensity seen below $q \approx 0.4c^*$ at low energies in (c) may be an artifact of imperfect background subtraction. From Zheludev et at.[109]

Fig. 12 shows the excitation spectrum close to $q = \pi$ at three fields bracketing the critical field. The energy range accessed includes only the easy plane modes and the field was applied in the easy plane. As expected the mode perpendicular to the field direction in the easy plane is driven down in energy, while the mode corresponding to fluctuations along the field direction stays constant up to the critical field. This behavior is consistent with perturbation theory based on the Wigner-Eckert theorem[110,111]. Above the critical field, the energy of the $||H$ mode is driven up as the system is magnetized, while the lower mode remains quasi-elastic. On general grounds it is to be expected that at $T = 0$ there should be a gap in the excitation spectrum above the critical field because the applied field in conjunction with the easy plane anisotropy leaves no continuous degree of freedom for the spin variables[77]. In order to remain in a disordered phase, the inelastic neutron scattering experiment was carried out at finite temperatures. Consequently the quasi-elastic scattering may correspond to scattering from thermally excited solitons as has previously been seen in high field experiments for classical easy plane antiferromagnets[112].

Low energy constant energy scans through $q = \pi$ show broadening beyond resolution in the high field phase. The characteristic Half Width at Half Maximum, κ, could either be associated with the thermal soliton density or it could be a measure of the deviation from half filling of a high field spinon Luttinger liquid. Further experiments will be required to distinguish between these two scenarios.

4 Conclusions

Zero field properties of integer and half odd integer spin chains are now well understood both from a theoretical and experimental standpoint. The spin-1/2 chain has gapless two-spinon continuum, while the spin-1 chain has a bound state that is separated from the singlet ground state by the Haldane gap. The magnetized state of the spin-1/2 chain has a new characteristic length scale that can be associated with the Fermi wave-vector of a one-dimensional Luttinger liquid shifted from half filling, or with the spacing between magnetized soliton defects. When there is a staggered g-tensor the magnetized state is in general gapfull and has transverse long range antiferromagnetic order. The spin-1 chain has a finite critical field that corresponds to closing the Haldane gap. However, when there is an alternating g-tensor, the gap actually never closes. Instead there is a cross-over from a low field phase with a Haldane gap to a high field phase with a residual gap induced by the staggered field. In addition transverse antiferromagnetic order is induced even for infinitesimal applied field. When there is no staggered field the high field phase should be gapless. Unfortunately most highly one-dimensional systems also have substantial spin space anisotropy. In our experiments on NDMAP the field was applied in the easy plane and so it may induce a gap in the $T = 0$ excitation spectrum. Instead we found quasi-elastic scattering at high fields and at temperatures above the phase transition

to static order. This quasi-elastic scattering may be associated with scattering from a thermally excited soliton gas.

An exciting experimental challenge that remains is to determine whether field induced incommensurate spin correlations occur in systems other than the spin-1/2 antiferromagnetic Heisenberg spin chain. The high field phase of the spin-1 chain would be an obvious place to look. Unfortunately the experiments are difficult because a gapless high field phase is only expected to exist in the high field limit when the field is applied perpendicular to an easy plane and when there is no staggered g-tensor. While NDMAP has no staggered g-tensor the proposed experiment is complicated by the fact that the magnetic field must be directed along the chain while at the same time wave-vector transfer must have a significant component along that direction. This geometry is incompatible with the conventional superconducting split coil magnet configuration where the field is perpendicular to the scattering plane. It appears that advances in high field magnet systems for neutron scattering or new model spin-1 chain systems will be needed for progress in this area.

Acknowledgements We thank R. Paul for help with neutron activation analysis. Work at JHU was supported by the United States National Science Foundation under DMR-9801742 and DMR-0074571. DHR acknowledges the support of the David and Lucile Packard Foundation. X-ray characterization and SQUID magnetometry was carried out using facilities maintained by the JHU MRSEC under NSF Grant number DMR-0080031. ORNL is managed by UT-Battelle, LLC for the U.S. DOE under contract DE-AC05-00OR22725. Work at BNL was carried out under DOE Contract No. DE-AC02-98CH10886. This work utilized neutron research facilities supported by NIST and the NSF under Agreement No. DMR-9986442.

References

1. M. Steiner, J. Villain, and C. G. Windsor, Adv. Phys. **25**, 87 (1976).
2. I. Affleck, J. Phys. Cond. Matt. **1**, 3047 (1989).
3. R. Chitra and T. Giamarchi, Phys. Rev B **55**, 5816 (1997).
4. J. Byrne, *Neutrons, Nuclei, and Matter, an exploration of the physics of slow neutrons*, Bristol, Philadelphia, Institute of Physics Publishing (1994).
5. S.M. Lovesey, *Theory of Thermal Neutron Scattering from Condensed Matter*, (Clarendon Press, Oxford) 1984.
6. P. J. Brown, in "International Tables for Crystallography", Volume C, edited by A. J. C. Wilson and E.Prince, Kluwer Academic Publishers Boston (1999).
7. H. Bethe, Z. Phys. **71**, 205 (1931).
8. M. Karbach and G. Müller, Comp. in Phys. **11**, 36-43 (1997); M. Karbach, K. Hu, and G. Müller, ibid **12** 565-573 (1998); M. Karbach, K. Hu, and G. Müller cond-mat/0008018 (2000).
9. L. Hulthén, Arkiv. Math Aston. Fysik **26A**, 11 (1938).
10. J. des Cloizeaux and J. J. Pearson, Phys. Rev. **128**, 2131 (1962).
11. J. Lowenstein, in *Recent Advances in Field Theory and Statistical Mechanics* Les Houches Summer School 1982 session XXXIX, edited by L. B. Zuber and R. Stora, North Holland, (1984).

12. L. Fadeev, in *Recent Advances in Field Theory and Statistical Mechanics* Les Houches Summer School 1982 session XXXIX, edited by L. B. Zuber and R. Stora, North Holland, (1984).
13. A. Luther and I Peshel, Phys. Rev. B **12**, 3908 (1975).
14. G. Müller, H. Thomas, H. Beck, and J. C. Bonner, Phys. Rev. B **24**, 1429 (1981).
15. S. M. Hayden, G. Aeppli, H. A. Mook, T. G. Perring, T. E. Mason, S.-W. Cheong, and Z. Fisk Phys. Rev. Lett. **76**, 1344 (1996).
16. J. M. Tranquada, B. J. Sternlieb, J. D. Axe, Y. Nakamura, and S. Uchida, NATURE **375** 561 (1995).
17. I. Zaliznyak *et al.*, to be published (2002).
18. N. Motoyama, N. Eisaki, and S. Uchida, Phys. Rev. Lett. **76** 3312 (1996).
19. I. A. Zaliznyak, C. Broholm, M. Kibune, M. Nohara, and H. Takagi, Phys. Rev. Lett. **83** 5370 (1999).
20. H. Suzuura, H. Yasuhara, A. Furusaki, N. Nagaosa, and Y. Tokura, Phys. Rev. Lett. **76**, 2579 (1996).
21. M. Takigawa, N. Motoyma, H. Eisaki, and S. Uchida, Phys. Rev. Lett. **76** 4612 (1996).
22. A. Keren, L. P. Le, G. M. Luke, B. J. Sternlieb, W. D. Wu, Y. J. Uemura, S. Tajima, and S. Uchida, Phys. Rev. B **48** 12926 (1993).
23. T. Ami, M. K. Crawford, R. L. Harlow, Z. R. Wang, D. C. Johnston, and Q. Huang, Phys Rev. B **51** 5994 (1995).
24. K. Yamada, J. Wada, S. Hosoya, Y. Endoh, S. Noguchi, S. Kawamata, K. Okuda, Physica C **253** 135 (1995).
25. A. Keren, K. Kojima, L. P. Le, G. M. Luke, W. D. Wu, Y. J. Uemura, S. Tajima, and S. Uchida, J. Magn. Mag. Mat. **140-144** 1641 (1995).
26. I. Tsukada, Y. Sasao, K. Uchinokura, A. Zheludev, S. Maslov, G. Shirane, K. Kakurai, and E. Ressouche Phys. Rev. B **60**, 6601 (1999).
27. I. Tsukada, J. Takeya, T. Masuda, and K. Uchinokura, Phys. Rev. B **62**, R6061 (2000).
28. M. Kenzelmann, A. Zheludev, S. Raymond, E. Ressouche, T. Masuda, P. Böni, K. Kakurai, I. Tsukada, K. Uchinokura, and R. Coldea Phys. Rev. B **64** 54422 (2001).
29. A. Zheludev, M. Kenzelmann, S. Raymond, T. Masuda, K. Uchinokura, S.-H. Lee, Phys. Rev. B **65**, 014402 (2002).
30. A. Zheludev, M. Kenzelmann, S. Raymond, E. Ressouche, T. Masuda, K. Kakurai, S. Maslov, I. Tsukada, K. Uchinokura, and A. Wildes Phys. Rev. Lett. **85**, 4799 (2000).
31. S. K. Satija, J. D. Axe, G. Shirane, H. Yoshizawa, and K. Hirakawa, Phys. Rev. B **21** 2001 (1980).
32. S. E. Nagler, D. A. Tennant, R. A. Cowley, T. G. Perring, and S. K. Satija, Phys. Rev. B **44** 12361 (1991).
33. M. T. Hutchings, E. J. Samuelsen, G. Shirane, and K. Hirakawa, Phys. Rev. **188** 919 (1969).
34. B. Lake, D. A. Tennant, and S. E. Nagler Phys. Rev. Lett. **85** 832 (2000).
35. D. A. Tennant, R. A. Cowley, S. E. Nagler, A. M. Tsvelik, Phys. Rev. B **52** 13368 (1995).
36. B. Grenier, L. P. Regnault, J. E. Lorenzo, J. P. Boucher, A. Hiess, G. Dhalenne, and A. Revcolevschi, Phys. Rev. B **62** 12206 (2000).
37. L. P. Regnault, M. Aïn, B. Hennion, G. Dhalenne, and A. Revcolevschi,Phys. Rev. B **53** 5579 (1996).
38. M. Arai, M. Fujita, M. Motokawa, J. Akimitsu, and S. M. Bennington, Phys Rev. Lett. **77** 3649 (1996).

39. Y. Endoh, G. Shirane, R. J. Birgeneau, P. M. Richards, and S. L. Holt, Phys. Rev. Lett. **32** 170 (1974).
40. I. U. Heilmann, G. Shirane, Y. Endoh, R. J. Birgeneau, and S. L. Holt, Phys. Rev. B **18** 3530 (1978).
41. D. C. Dender, P. R. Hammar, D. H. Reich, C. Broholm, and G. Aeppli, Phys. Rev. Lett. **79** 1750 (1997)
42. D. C. Dender, D. Davidović, D. H. Reich, C. Broholm, Phys. Rev. B **53** 2583 (1996).
43. Y. Chen, Johns Hopkins University, PhD. Thesis.
44. C. P. Landee, A. C. Lamas, R. E. Greeney, K. G. Bücher, Phys. Rev. B **35** 228 (1987).
45. P. R. Hammar, M. B. Stone, D. H. Reich, C. Broholm, P. J. Givson, M. M. Turnbull, C. P. Landee, and M. Oshikawa, Phys. Rev. B **59** 1008 (1999).
46. R. Coldea, D. A. Tennant, R. A. Cowley, D. F. McMorrow, B. Dorner, and Z. Tylczynski, Phys. Rev. Lett. **79** 151 (1997).
47. M. W. VanTol and N. J. Poulis, Physica **69** 341 (1973).
48. J. P. Groen, T. O. Klaassen, N. J. Poulis, G. Müller, H. Thomas, and H. Beck, Phys. Rev. B **22** 5369 (1980).
49. W. E. Hatfield, W. E. Estes, W. E. Marsh, M. W. Pickens, L. W. ter Haar, and R. R. Weller, in *Extended Linear Chain Compounds*, edited by J. S. Miller (Plenum, New York, NY 1983), p. 43.
50. L. J. de Jongh and A. R. Miedema, Adv. in Phys. **23** 1 (1974).
51. D. A. Tennant, R. A. Cowley, S. E. Nagler, and A. M. Tsvelik, Phys. Rev. B **52**, 13368 (1995).
52. M. B. Stone *et al.*, to be published (2002).
53. G. Müller, H. Beck, and J. C. Bonner, Phys. Rev. Lett. **43**, 75 (1979).
54. M. Karbach, G. Muller, A. H. Bougourzi, A. Fledderjohann, and K. H. Mutter Phys. Rev. B **55**, 12510 (1997).
55. A. J. Millis, Private Communications (1997).
56. I. Affleck and M. Oshikawa, Phys. Rev. B **60**, 1038 (1999).
57. F. H. M. Essler and A. M. Tsvelik, Phys. Rev. B **57**, 10592 (1998).
58. M. Oshikawa and I Affleck, Phys. Rev. Lett. **79** 2883 (1997).
59. E. Pytte, Phys. Rev. B **10**, 4637 (1974); M. C. Cross and D. S. Fischer, Phys. Rev. B **19**, 402 (1979); J. W. Bray, L. V. Interrante, I. S. Jacobs, and J. C. Bonner, in *Extended Linear Chain Compounds*, edited by J. S. Miller (Plenum, New York, 1982), Vol. 3, pp. 353-415.
60. A. I. Buzdin, M. L. Kulic and V. V. Tugushev, Solid State Comm. **48**, 483 (1983).
61. M. Fujita and K. Machida, J. Phys. C: Solid State Phys. **21**, 5813 (1988).
62. H. M. Rønnow, M. Enderle, D. F. McMorrow, L. P. Regnault, G. Dhalenne, A. Revcolevschi, A. Hoser, K. Prokes, P. Vorderwisch and H. Schneider, Phys. Rev. lett. **84**, 4469 (2000).
63. V. Kiryukhin, B. Keimer, J. P. Hill and A. Vigliante, Phys. Rev. Lett. **76**, 4608 (1996).
64. M. Enderle, H. M. Rønnow, L. P. Regnault, G. Dhalenne, A. Revcolevschi, P. Vorderwisch, H. Schneider, P. Smeibidl and M. Meissner, Phys. Rev. Lett. **87**, 177203 (2001).
65. F. D. M. Haldane, Phys. Lett. **93A**, 464 (1983).
66. F. D. M. Haldane, Phys. Rev. Lett., **50**, 1153 (1983).
67. E. Lieb, T. D. Schultz, and D. C. Mattis, Ann. Phys. **16**, 407 (1962).
68. M. Yamanaka, M. Oshikawa, and I. Affleck, Phys. Rev. Lett., **79**, 1110 (1997).

69. M. Oshikawa Phys. Rev. Lett. **84**, 3370 (2000).
70. M. P. Nightingale and H. W. J. Blöte, Phys. Rev. B **33** 659 (1986).
71. S. R. White and D. A. Huse, Phys. Rev. B **48** 3844 (1993).
72. I. Affleck, T. Kennedy, E. H. Lieb, and H. Takaki, Phys. Rev. Lett. **59**, 799 (1987).
73. D. P. Arovas, A. Auerbach, and F. D. M. Haldane, Phys. Rev. Lett., **60**, 531 (1988).
74. M. den Nijs and K. Rommelse, Phys. Rev. B **40**, 4709 (1989).
75. F. C. Alcaraz and Y. Hataugai, Phys. Rev. B **46**, 13914 (1992).
76. R. Scharf and H.-J. Mikeska, J. Phys. Cond. Matt., **7**, 5083 (1995).
77. I. Affleck, Phys. Rev. B **41**, 6697 (1990); Phys. Rev. B **43**, 3215 (1991).
78. H. Mutka, J. L. Soubeyroux, G. Bourleaux and P. Colombet, Physica B **39**, 4820 (1989).
79. J. Darriet and L. P. Regnault, Solid State Commun. 86, 409 (1993).
80. J. F. DiTusa, S-W. Cheong, J. -H. Park, G. Aeppli, C. Broholm, and C. T. Chen, Phys. Rev. Lett. **73**, 1857 (1994).
81. Guangyong Xu, J. F. DiTusa, T. Ito, K. Oka, T. Ito, H. Takagi, C. Broholm, and G. Aeppli, Phys. Rev. B **54**, 6827 (1996).
82. A. Zheludev, S. E. Nagler, S. M. Shapiro, L. K. Chou, D. R. Talham, and M. W. Meisel, Phys. Rev. B **53**, 15004 (1996).
83. J. P. Renard, V. Gadet, L. P. Regnault, and M. Verdaguer, J. Magn. Magn. Mater. 90, 213 (1990).
84. L. K. Chou, D. R. Talham, W. W. Kim, P. J. C. Signore, and M. W. Meisel, Physica B **194-196**, 313 (1994).
85. J. P. Renard, M. Verdaguer, L. P. Regnault, W. A. C. Erkelens, J. Rossatmignod, J. Ribas, W. G. Stirling, and C. Vettier, J. Appl. Phys. **63**, 3538 (1988).
86. K. Hirota, S.M. Shapiro, K. Katsumata, and M. Hagiwara, Physica B **213**, 173 (1995).
87. Shaolong Ma, Collin Broholm, Daniel H. Reich, B. J. Sternlieb, and R. W. Erwin, Phys. Rev. Lett. **69**, 3571 (1992).
88. L. P. Regnault, I. Zaliznyak, J. P. Renard, and C. Vettier Phys. Rev. B **50**, 9174 (1994).
89. O. Avenel it et al., Phys. Rev. B **46**, 8655 (1992).
90. Z. Honda, H. Asakawa, and K. Katsumata, Phys. Rev. Lett. **81**, 2566 (1998).
91. Y. Chen, Z. Honda, A. Zheludev, C. Broholm, K. Katsumata, and S. M. Shapiro, Phys. Rev. Lett. **86**, 1618 (2001).
92. A. Zheludev, Y. Chen, C. L. Broholm, Z. Honda, and K. Katsumata, Phys. Rev. B **63**, 104410 (2001).
93. Y. Koike, M. Metoki, Y. Morii, T. Kobayashi, T. Ishii, M. Yamashita, J. Phys. Soc. Jpn. **69**, 4034 (2000).
94. A. Zheludev, Y. Chen, C. L. Broholm, Z. Honda, K. Katsumata, Phys. Rev. B **63**, 104410 (2001).
95. Rose M. Morra, William J. L. Buyers, Robin L. Armstrong and K. Hirakawa, Phys. Rev. B **38**, 543 (1988).
96. W. J. L. Buyers, R. M. Morra, R. L. Armstrong, M. J. Hogan, P. Gerlach and K. Hirakawa, Phys. Rev. Lett. **56**, 371 (1986).
97. M. Takahashi, Phys. Rev. Lett. **62**, 2313 (1989).
98. K. Nomura, Phys. Rev. B **40**, 2421 (1989).
99. S. Liang, Phys. Rev. Lett. **64**, 1597 (1990).
100. J. P. Renard, M. Verdaguer, L. P. Regnault, W. A. C. Erkelens, J. Rossatmignod, and W. G. Stirling Europhys. Lett. **3**, 945 (1987).
101. P. C. Hohenberg and W. F. Brinkman, Phys. Rev. B **10**, 128 (1974).

102. S. M. Girvin, A. H. MacDonald and P. M. Platzman, Phys. Rev. B **33**, 2481 (1986).
103. I. Zaliznyak, S.-H. Lee and S. V. Petrov, Phys. Rev. Lett. **87**, 017202 (2001).
104. M. Enderle, L. P. Regnault, C. Broholm, D. H. Reich, I. Zaliznyak, M. Sieling, H. Ronnow, and D. F. McMorrow PHYSICA B **276** 560-561 (2000).
105. M. Sieling, U. Low, B. Wolf, S. Schmidt, S. Zvyagin, and B. Luthi Phys. Rev. B **61**, 88 (2000).
106. A. Zheludev, Z. Honda, K. Katsumata , R. Feyerherm and K. Prokes, Europhys. Lett. **55**, 868 (2001).
107. Z. Honda, H. Asakawa, and K. Katsumata, Phys. Rev. Lett. **81**, 2566 (1998).
108. Z. Honda, K. Katsumata, Y. Nishiyama, and I. Harada, Phys. Rev. B **63**, 064420 (2001).
109. A. Zheludev, Z. Honda, Y. Chen, C. L. Broholm, K. Katsumata, S. M. Shapiro, Phys. Rev. Lett **88**, 077206 (2002).
110. O. Golinelli, T. Jolicoeur, and R. Lacaze, J. Phys. Condens. Matter **5**, 7847 (1993).
111. L.-P. Regnault, I. A. Zaliznyak and S. V. Meshkov, J. Phys. Condens. Matter **5**, L677 (1993).
112. H. J. Mikeska and M. Steiner, Adv. in Phys. **40**, 191 (1991).